RAA 2019 Vol. **19** No. **2**, 19(14pp) doi: 10.1088/1674–4527/19/2/19

http://www.raa-journal.org *http://iopscience.iop.org/raa*

***R**esearch in*
***A**stronomy and*
***A**strophysics*

Prospects for detecting ultra-high-energy particles with FAST

Clancy W. James[1], Justin D. Bray[2] and Ronald D. Ekers[3]

[1] International Centre for Radio Astronomy Research, Curtin University, GPO Box U1987, Perth, WA 6845, Australia; ARC Centre of Excellence for All-Sky Astrophysics (CAASTRO); *clancy.james@curtin.edu.au*
[2] School of Physics & Astronomy, University of Manchester, Manchester M13 9PL, United Kingdom
[3] CSIRO Astronomy & Space Science, PO Box 76, Epping, NSW 1710, Australia

Received 2018 February 6; accepted 2018 June 5

Abstract The origin of the highest-energy particles in nature, ultra-high-energy (UHE) cosmic rays, is still unknown. In order to resolve this mystery, very large detectors are required to probe the low flux of these particles — or to detect the as-yet unobserved flux of UHE neutrinos predicted from their interactions. The 'lunar Askaryan technique' is a method to do both. When energetic particles interact in a dense medium, the Askaryan effect produces intense coherent pulses of radiation in the MHz–GHz range. By using radio telescopes to observe the Moon and look for nanosecond pulses, the entire visible lunar surface (20 million km^2) can be used as a UHE particle detector. A large effective area over a broad bandwidth is the primary telescope requirement for lunar observations, which makes large single-aperture instruments such as the Five-hundred-meter Aperture Spherical radio Telescope (FAST) well-suited to the technique. In this contribution, we describe the lunar Askaryan technique and its unique observational requirements. Estimates of the sensitivity of FAST to both the UHE cosmic ray and neutrino flux are given, and we describe the methods by which lunar observations with FAST, particularly if equipped with a broadband phased-array feed, could detect the flux of UHE cosmic rays.

Key words: cosmic rays — neutrinos — techniques: miscellaneous — Moon

1 INTRODUCTION

Ultra-high-energy (UHE) cosmic rays are the highest-energy particles in nature, with a flux extending up to at least 100 EeV (10^{20} eV). Their origin remains unknown, largely due to the bending of their trajectories in cosmic magnetic fields. Only at extreme energies above 10^{18} eV have these particles been shown to retain some directional information, as first shown by a tentative correlation of the arrival directions of these particles with nearby active galactic nuclei (AGN) (Pierre Auger Collaboration et al., 2007). However, the AGN used for the correlation mostly serve as proxies for the large-scale matter distribution in the local universe, and the correlation remains weak (Abreu et al., 2010). The statistically strongest result is that of a weak dipole anisotropy indicating an extragalactic origin (Pierre Auger Collaboration et al., 2017), but not what that origin is.

The reason why the source(s) of the UHE cosmic rays cannot be identified is simple: in this energy range, the flux is approximately one particle per square kilometre per century, so that even the 3000 km^2 Pierre Auger Observatory in Argentina only detects of order 30 particles above 5.6×10^{19} eV per year (the energy at which the greatest correlation with AGN was found). In order to determine the origin of these particles, an even larger detector is required. However, the cost of building such a detector in the style of the Pierre Auger Observatory has so-far proved too great, motivating the use of new techniques.

Another method to determine the cosmic-ray origin is to detect the neutrinos produced from cosmic-ray interactions with background photon fields, and/or any flux expected from their interactions during acceleration (Beresinsky & Zatsepin, 1969). Since neutrinos are uncharged and weakly interacting, any high-energy neutrino flux will arrive at Earth directly from the source, so that detecting this flux should point back to the source of the UHE cosmic rays, thus giving another method to resolve the UHE cosmic-ray mystery.

The lunar Askaryan technique (Dagkesamanskii & Zheleznykh 1989) is a method to detect both the highest-energy cosmic rays and neutrinos, using the Askaryan effect (Askaryan 1962, 1965). Askaryan predicted that a particle cascade in a medium would develop an excess of negative charge due to the entrainment of atomic electrons and the annihilation of positrons in-flight. This excess charge — of order 10% of the total charge — will radiate coherently at wavelengths comparable to the dimensions of the cascade. Thus, the total power radiated will scale with the square of the excess charge, and hence with the square of the primary particle energy. Experiments utilising the Askaryan effect therefore tend to target the highest-energy particles. Cosmic rays impacting the Moon will produce cascades approximately 10 cm wide and a few metres long (Alvarez-Muñiz et al. 2006), so that coherent radiation is expected in the 100 MHz to a few GHz regime. By observing the Moon with a ground-based radio telescope, its entire visible surface of twenty million square kilometres can be used as a cosmic ray detector.

The Askaryan effect has since been confirmed via accelerator experiments at SLAC (Saltzberg et al. 2001), and numerous experiments have utilised the lunar Askaryan technique to search for UHE particles impacting the Moon. These have covered observations at Parkes and the ATCA by the LUNASKA collaboration (Hankins et al. 1996; James et al. 2010); GLUE at Goldstone (Gorham et al. 2004); a series of observations using the telescope at Kalyazin (Beresnyak et al. 2005); the NuMoon project's observations with the WSRT (Buitink et al. 2010); and RESUN at the VLA/EVLA (Jaeger et al. 2010). While these experiments made significant advances in the unique techniques required to detect Askaryan radiation, none had the sensitivity to identify the signature pulses produced by such particle interactions.

The Square Kilometre Array (SKA) is a next-generation radio telescope shortly to begin Phase 1 construction. One of the two main science goals of the SKA's High Energy Cosmic Particles Focus Group is to harness the power of the SKA for lunar Askaryan observations (Bray et al. 2015). However, due to the reduced sensitivity of Phase 1 of the SKA, over 1000 h will likely be required per detected event. This leaves a critical window for the Five-hundred-meter Aperture Spherical radio Telescope (FAST) to make a first detection of the UHE cosmic ray flux with the lunar Askaryan technique.

In Section 2, the radio emission from particle cascades in the Moon is described, outlining the basic properties of the signal produced by UHE cosmic ray and neutrino interactions. The unique observing mode required to detect such a signal is described in Section 3, focussing in particular on dedispersion, radio frequency interference (RFI) discrimination and triggering. The expected sensitivity of FAST to UHE cosmic rays and neutrinos using the lunar Askaryan technique is simulated in Section 4, using a detailed Monte Carlo code developed for the LUNASKA experiments at Parkes and the ATCA. Using these results, we discuss the potential of the lunar Askaryan technique with FAST in regards to UHE particle searches in Section 5.

2 RADIO EMISSION FROM UHE PARTICLES IMPACTING THE MOON

When a high-energy particle interacts in a medium, it produces a cascade of secondaries with initially balanced positive and negative charges. Compton, Moeller and Bhabha scattering of medium electrons (by gamma rays, electrons and positrons, respectively) will entrain medium electrons into the cascade, while occasionally cascade positrons will annihilate in-flight. As predicted by G. A. Askaryan, these processes produce a total negative charge excess of order 10%. An observer will see this charge excess rapidly appear and disappear as a sudden 'flash', producing a pulse of radiation lasting no longer than the duration of the cascade as seen by an observer. This 'Askaryan radiation' will therefore be coherent at wavelengths greater than the apparent size of the cascade. At the Cherenkov angle ($\theta_C = \cos^{-1} n^{-1}$, where n is the refractive index), emission along the entire length of the cascade will radiate coherently, and coherency will be limited only by the width of the cascade[1]. At angles far from θ_C however, high-frequency radiation along the length of the cascade will tend to destructively interfere, and coherency will be observed only at lower frequencies.

Cosmic rays impacting the Moon will produce hadronic cascades in the lunar regolith, the outer-most layer of sand-like material covering the Moon. This material has an approximate density of $\rho \sim 1.8$ g cm^{-3} (Olhoeft & Strangway 1975), producing cascades which are $\sim$ 10 cm wide and a few metres long (Alvarez-Muñiz et al. 2006). Therefore, emission from lunar cascades can peak in the GHz regime. The expected emission from a 10^{20} eV hadronic cascade in the lunar regolith at 300 MHz and 1 GHz is shown by the black 'intrinsic' lines in Figure 1, as a function of the angle from the shower axis (for more details on signal simulation, see Sect. 4).

[1] Although the peak emission is at the Cherenkov angle, the radiation arising from the Askaryan effect is not simply Cherenkov radiation — see the appendix of James et al. (2011a) for a discussion.

The 1 GHz emission is stronger, but the 300 MHz emission broader.

The emission that escapes the regolith to be seen by an observer however is strongly dependent on the interaction geometry. Since the Cherenkov angle is the complement of the angle of total internal reflection, the peak emission from cascades parallel to the surface will not escape the regolith. This is shown by the blue 'ν' lines in Figure 1. Since cosmic rays will always interact pointing into the surface, the suppression due to transmission effects is even greater, as shown by the red 'CR' line in Figure 1. At high frequencies therefore, only those cosmic rays impacting the surface at low incident angles will be visible. These transmission effects also mean that an observer will preferentially observe radiation coming from the lunar limb, especially at higher frequencies — this is often termed the 'limb brightening' effect.

The Askaryan radiation emitted from particle cascades is always linearly polarised in the plane of the observer and the shower axis. Radiation escaping the surface will thus tend to be polarised parallel to the local surface normal. Combined with the limb-brightening effect, Askaryan pulses from UHE particles hitting the Moon will tend to appear as linearly-polarised, bandwidth-limited impulses with polarisation pointing radially outward from the Moon.

The emission from UHE neutrino-induced cascades will appear similarly to that from cosmic-ray-induced cascades, with a few important differences. Firstly, neutrinos will only deposit of order 20% of their energy as hadronic cascades. In neutral-current (NC) interactions, the remaining 80% will be carried away by the neutrino, while the lepton produced in charged-current (CC) interactions will deposit its energy over a large distance, producing almost no visible emission. Unlike cosmic rays, neutrinos can penetrate a large fraction of the Moon before interacting (interaction length of 216 km water equivalent at 10^{20} eV; Gandhi et al. (1998)). While they will not pass through the entire Moon, they can 'skim' the outer layers, and interact near the surface so that the resulting cascade points upwards, allowing high-frequency emission to escape. However, the majority of neutrinos will interact too deeply in the Moon to produce visible radiation. The absorption length is such that the emitted field strength E at frequency f reduces approximately as: $E \sim \exp\{-(d/18\,\mathrm{m})(f/1\,\mathrm{GHz})\}$ for an interaction at depth d, so that the interaction volume accessible at low frequencies is greater. Note that while the 'lunar regolith' (of $2-10$ m thickness; Shkuratov & Bondarenko (2001)) is often used as shorthand for the lunar material with which UHE particles will interact, in fact all lunar rock should be relatively radio-transparent, so the depth of the regolith layer will not limit the interaction volume of UHE neutrinos. Example pulses are shown in Figure 2.

The most important effect of lunar topology on the Askaryan emission from both types of particle cascades is that of the rough lunar surface, as shown in Figure 3. On large scales, surface features such as craters and hills will tend to cause cosmic rays to interact pointing into the local surface, so the radiation is directed into the Moon. On small scales, roughness over the area through which the radiation exits the Moon can cause decoherence effects. These effects will be larger for neutrino interactions, where the outgoing radiation transmits through a larger portion of the surface. The exact effects of lunar surface roughness are the least well understood aspect of the theory of lunar Askaryan emission.

In the next section, the basic strategy for detecting these ultra-short signals using a large single-dish telescope such as FAST is described.

3 OBSERVATIONAL REQUIREMENTS

Observing lunar Askaryan pulses with a conventional radio telescope presents a unique challenge. The signal must be sampled at full time resolution, and searched for an excess of impulse-like events. The signal must be dedispersed in order to compensate for the phase delays induced by the Earth's ionosphere, and lunar pulses must be distinguished from impulsive RFI and thermal noise fluctuations. The more general requirements of an observation are described below, followed by a detailed description of these specialised requirements in their respective subsections.

The principle of searching for lunar Askaryan pulses with a ground-based radio telescope is relatively simple: point the telescope at the Moon and search for nanosecond pulses. The coherence of the radiation means that the sensitivity scales linearly with both antenna effective area and the available bandwidth. The relevant frequency range is from approximately 100 MHz, below which the emission will be too weak to detect, up to approximately 2 GHz, above which the radiation is emitted over such a narrow angular range that the probability of detection is too low. The proposed ultra-wideband single-pixel feed (SPF; Li et al. (2013)), with a potential bandwidth from 270 MHz to 1.45 GHz, will thus provide the greatest sensitivity per beam for lunar observations, with bandwidth-area product of order 60 000 m^2 GHz, compared to the previous maximum of $\sim$1300 m^2 GHz for the first Parkes experiment (Hankins et al. 1996).

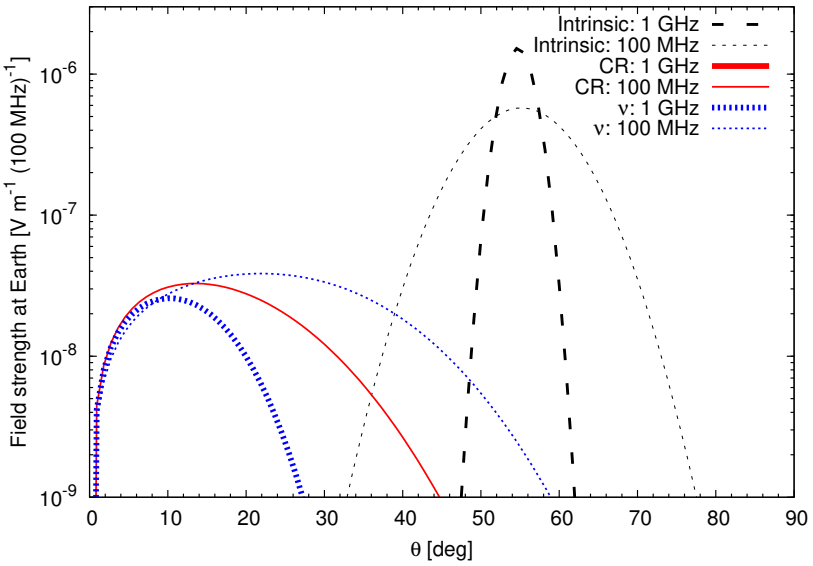

Fig. 1 Spectral radiation strength at Earth from 10^{20} eV particle interactions in the lunar regolith, at 1 GHz (*thick*) and 300 MHz (*thin*), as a function of angle with respect to the lunar surface. *Black* 'intrinsic': emission from a cascade parallel to the surface (direction $\theta = 0$), ignoring absorption in, and refraction and transmission through, the lunar surface. Note the peak at the Cherenkov angle of $55°$. *Red* 'CR': characteristic emission of a cosmic ray directed $10°$ into the lunar surface — the 1 GHz emission is not visible on this scale. *Blue* 'ν': characteristic emission of a neutrino parallel to the surface, at depth of 10 m, giving only 20% of its energy to a particle cascade.

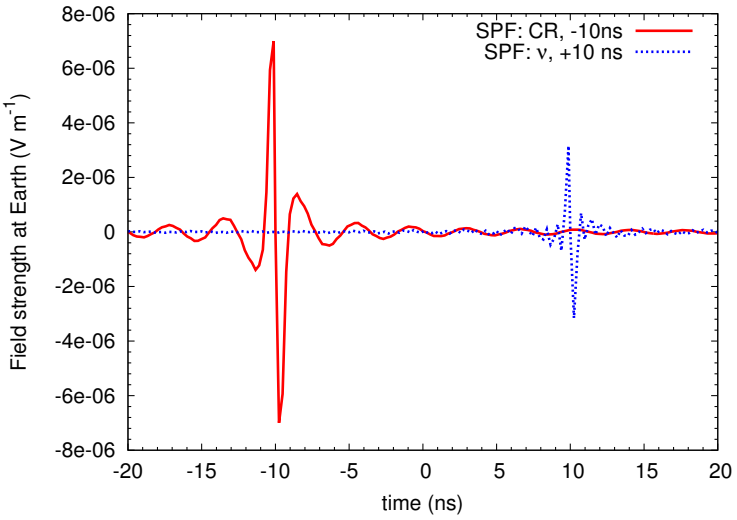

Fig. 2 Time-domain signals of the characteristic cosmic ray (CR: *red*) and neutrino (ν: *blue dotted*) events shown in Fig. 1 as viewed from Earth. The assumed emission angle is $5°$, and the bandwidth is 270 MHz to 1.45 GHz. The curves are offset by ± 10 ns for clarity.

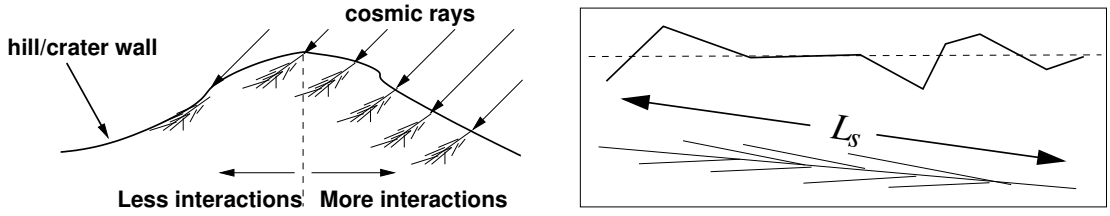

Fig. 3 Sketches indicating the effects of lunar surface roughness. Left: cosmic rays will tend to interact on backwards-sloping surface features, making the escape of radiation more difficult. Right: roughness (*solid line*) on scales comparable to the length L_s of a particle shower will scatter and reduce the coherence of out-going radiation compared to emission through a smooth surface (*dashed*).

As much of the lunar disc (diameter $\sim 30'$) as possible should be observed simultaneously in order to maximise the event rate, or at least the lunar limb, due to the 'limb brightening' effect (Sect. 2). In the GHz regime, the FAST beam however is very small compared to the Moon, which is the main disadvantage of using a single beam from a single large dish for lunar observations. The 19-beam FAST multibeam receiver (Nan et al., 2011) will somewhat alleviate this problem, albeit with a smaller bandwidth of $1.23 - 1.53\,\mathrm{GHz}$[2].

A possible observing configuration for both the multibeam and SPF is shown in Figure 4. The multibeam configuration allows four on-limb beams (b2, b3, b16 and b19), which will be the most sensitive to Askaryan signals, while the optimal SPF pointing is $0.44'$ off-limb. Such a slight off-limb pointing tends to be advantageous because the noise in each beam will be dominated by lunar thermal emission, at approximately 225 K (Troitskij & Tikhonova 1970). Pointing slightly off-limb thus significantly reduces the lunar noise contribution while maintaining sensitivity to the majority of signal events.

The small angular coverage of standard receivers, combined with the dominance of lunar noise, makes a phased-array feed (PAF) well-suited for lunar observations. In the ideal case, a PAF could be built which would simultaneously observe the entire lunar disc over a bandwidth comparable to that of the SPF, without too great an increase in system temperature. While the building of such a receiver would be challenging, it would also be useful for other FAST observation programs, such as pulsar searches.

Regardless of which beam is used, the special requirements of dedispersion, RFI discrimination and the likely management of a high data rate via triggering, will have to be implemented. These are described below.

3.1 Dedispersion

The broad bandwidth and short time-duration of Askaryan pulses mean that the dispersion induced by Earth's ionosphere is significant. Since the main characteristic of the pulses is their short time-duration, any signal smearing due to dispersion over the observation bandwidth will drastically reduce the experimental sensitivity. The dispersion Δt induced in a pulse can be calculated via Equation (1)

$$\Delta t(\mathrm{s}) \;=\; 1.34 \times 10^{-3}\,\mathrm{STEC}\,\left(f_{\mathrm{min}}^{-2} - f_{\mathrm{max}}^{-2}\right)\;, \quad (1)$$

where f_{min} and f_{max} are the minimum and maximum observation frequencies (Hz) respectively, and STEC is the slant total electron content ($\mathrm{e}^-\,\mathrm{cm}^{-2}$) along the line of sight. For a bandwidth of 1.23 to 1.53 GHz, and typical night-time STEC of $7\times10^{12}\,\mathrm{e}^-\,\mathrm{cm}^{-2}$, the pulse is smeared over $\Delta t = 2.2$ ns, which is comparable to the inverse bandwidth. During the day, or during periods of significant solar activity, the dispersion will be greater. The effects over broader bandwidths, and at lower frequencies, will also be greater. An example of dispersive effects is given in Figure 5 (left), in the case of a 270 MHz–1.43 GHz bandwidth and STEC of 7×10^{12}. This can be compared to the measured VTEC (vertical TEC, equal to STEC only for a source at zenith) at the FAST site, with monthly averages for 2007 (during a solar minimum) shown in Figure 5 (right). While dispersion can be compensated for in digital signal processing, its accuracy is limited by knowledge of the Earth's ionosphere at the telescope location, so that ionospheric monitoring is vital to the success of the experiment.

The necessary real-time monitoring and correction has been successfully used at the LUNASKA experiment at Parkes (Bray et al. 2013b), thus demonstrating the feasibility of this method, albeit only over the $1.23 - 1.53$ GHz band. It may be possible however to use the Faraday rotation of the polarised component of the emission of the Moon itself to determine the dispersion along the line-of-sight (McFadden et al. 2012).

3.2 RFI Discrimination

Askaryan pulses appear very similar to bandwidth-limited impulses. Two types of events can imitate the signal: random noise fluctuations and short-time-duration RFI, both of which must be excluded in order to identify a lunar Askaryan signal. Rejecting the former is simply a matter of setting a sufficiently high detection threshold, although the exact noise statistics can become quite complex (Bray et al. 2013a). For radio-telescope arrays, rejecting RFI also becomes relatively easy, since the angular resolution of arrays readily allows signals not of lunar origin to be rejected. For single-dish experiments such as FAST however, RFI discrimination becomes much more difficult. The methods developed by the LUNASKA experiment at Parkes (Bray et al. 2013b) will be equally applicable at the FAST telescope and are discussed below.

RFI that can imitate an Askaryan pulse is necessarily broadband and of short time duration. Unlike the narrowband RFI environment at radio-telescope facilities, which tends to be well-monitored, sources of impulsive RFI are largely unknown. Examples found in the Parkes experiment include air conditioners in the control room and

[2] The expected receiver bandwidth has now been changed to $1.05 - 1.45$ GHz (D. Li, private communication).

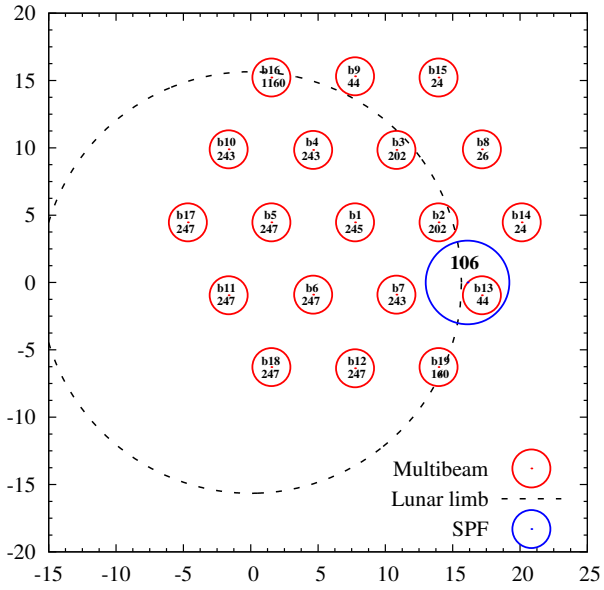

Fig. 4 Configuration of simulated FAST beams compared to the Moon, at distance 3.844×10^8 m. *Red*: central positions of the 19 beams of the multi-beam receiver; *blue*: assumed pointing position of the single-pixel wideband feed. The estimated $T_{\rm sys}$ of each beam is also shown. The beam size is calculated at the geometric mean of the bandwidth, i.e. $(f_{\rm min} f_{\rm max})^{0.5}$, while $T_{\rm sys}$ is averaged over the band.

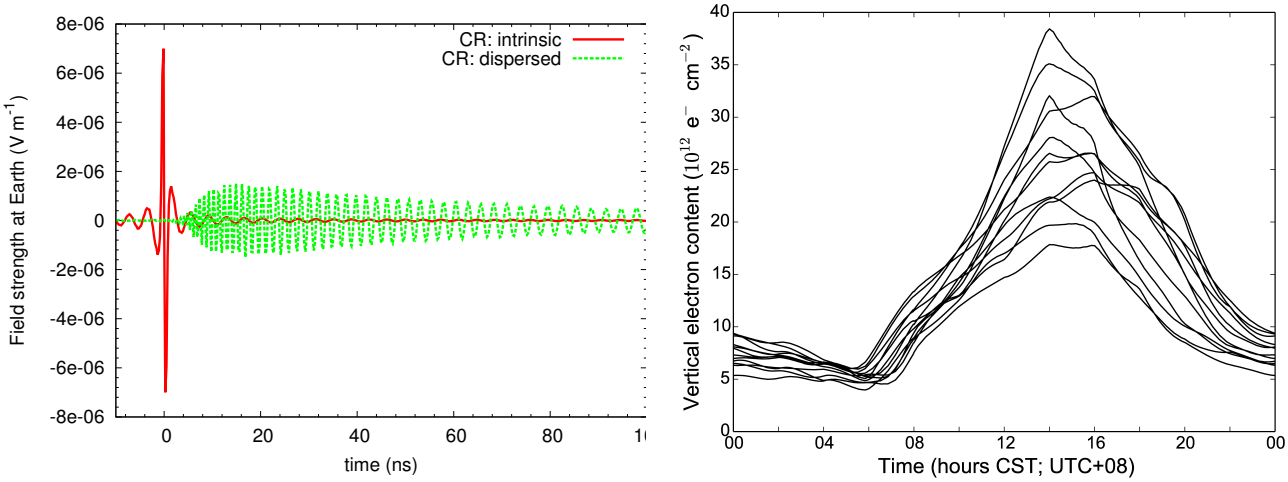

Fig. 5 *Left*: effects of dispersion (*green dashed line*) on an example cosmic-ray signal (*solid red line*). The assumed bandwidth is 270 MHz–1.43 GHz with STEC of 7×10^{12} e$^-$ cm^{-2}. *Right*: monthly-averaged VTEC values for 2007 at the FAST site as a function of local time (CST), as derived from GPS data (Noll, 2010).

noise-calibration diodes located in the telescope receiver. Such pulses will differ from true lunar pulses in the following ways: their origin, their polarisation, their timing and their lack of an atmospheric dispersion signature. Of these, the signal polarisation does not generally provide a strong discriminant, since the expected polarisation of lunar signals can only be approximately predicted (and at low frequencies, will be Faraday-rotated over the bandwidth). The expected dispersion signature is however a strong discriminant — terrestrial RFI will obviously not be dispersed, unless it is reflected off an object outside the atmosphere, in which case it will be doubly dispersed. RFI also tends to arrive in bursts and is usually longer in duration than Askaryan pulses, so that the high time resolution required to search for the pulses also helps discriminate against RFI events. The strongest discriminant used in the Parkes experiment however was the required lunar origin, using an anti-coincidence veto between different beams on the multibeam receiver.

Lunar-origin pulses are point-like events, and all but the most energetic events will appear in at most one beam of a multi-beam receiver. Terrestrial RFI however will not enter through the main telescope beams and will tend to appear in multiple beams at once. Events appearing in more than one beam therefore will likely not be lunar in origin. Any beams pointing away from the Moon (such as beams 8, 14 and 15 in Figure 4) will have a lower system temperature and therefore be especially sensitive to RFI events. Similar methods would also apply to beams formed from the elements of a PAF — in the case of an SPF however, no equivalent method could be used, so that RFI discrimination would be much more difficult.

3.3 Triggering

The lunar Askaryan technique involves searching for a signal which closely resembles a bandwidth-limited impulse, being only nanoseconds in duration. Therefore, the full time resolution of the telescope must be preserved, since any averaging — or splitting of the bandwidth — will dilute the signal power. The bandwidth must also be sampled at high precision, in order to simultaneously determine the rms noise voltage and provide a sufficient dynamic range for signal detection. For the FAST multibeam, with two polarisation channels per beam, each sampled at $\sim 1.024\,\mathrm{GHz}$ with 8-bit precision, the data rate would be approximately $40\,\mathrm{GB\,s^{-1}}$. If this is too high for baseband recording to be practical, a real-time trigger must be implemented to detect likely candidate pulses in real time and record snapshots of the data. Such a trigger method has been used in all previous searches for lunar pulses, with the exception of the NuMoon observations at Westerbork.

A real-time trigger will inevitably not be as sensitive to lunar pulses as a full offline analysis could be. In the case of a radio-telescope array, the main challenge is to combine information from several antennas in real-time to form a trigger, which is the biggest advantage of a single-dish experiment such as FAST over such instruments. Dedispersion in real-time however can prove difficult, both computationally and because information on the total electron content along the telescope line-of-sight is often not immediately available. Effects on the signal due to a finite sampling rate, and phase randomisation due to downconversion, may also need to be corrected for (Bray et al., 2012), which again is more difficult in real time.

To compensate for imperfect sensitivity, the threshold of a real-time trigger can be set well below the theoretical signal detection threshold, producing a high rate of candidate events to ensure that any signal event is recorded. The optimal trigger rate depends on the dead-time of the system upon triggering, which in turn depends on the amount of data that must recorded for each trigger. As discussed above, single-dish experiments such as FAST typically have trouble discriminating against terrestrial RFI. While the anti-coincidence method rejects almost all impulsive RFI with high accuracy, it may be necessary to record microseconds' worth of data from all beams upon each trigger in order to help discriminate against the small fraction of RFI that remains.

All the above methods — dedispersion, RFI discrimination and triggering — were used in the LUNASKA experiment at Parkes to reach a sensitivity very close to the thermal noise level (Bray et al., 2013b), indicating that this will also be possible at FAST (at least in the case of a multibeam or PAF receiver). We therefore proceed to simulate the sensitivity of a lunar Askaryan experiment at FAST on the assumption that the limiting sensitivity of the thermal noise level can be reached. For a review of effects which have reduced the sensitivity of past experiments, see Bray (2016).

4 SIMULATIONS

Simulations of UHE particle interactions in the Moon, and the associated radio-wave production and propagation, were performed by a detailed Monte Carlo code (James & Protheroe 2009b). The program interacts UHE particles with the Moon, calculates the radiation strength using parameterisations based on Monte Carlo simulations of particle cascades (Zas et al. 1992; Alvarez-Muñiz & Zas 1998; Alvarez-Muñiz et al. 2006), accounts for transmission through, and absorption in, the rough lunar surface, and determines if the signal is detectable by a simulated instrument. The accuracy of the simulation has been confirmed by analytic calculations (Gayley et al. 2009). Note that while the simulation implicitly assumes cosmic-ray primaries to be protons (the parameterisations on which they are based are made with protons), the resulting emission will be highly insensitive to the nature of the primary particle, since the mechanisms producing an excess charge — and hence Askaryan emission — in particle cascades become important only below $\sim 100\,\mathrm{MeV}$ (Zas et al. 1992), and the total electromagnetic fraction is a weak function of primary nucleon energy (Alvarez-Muñiz & Zas 1998).

The main uncertainty in simulating the signal from cosmic-ray interactions comes from the interaction of the cosmic rays with lunar surface features, which tend to cause cascades to occur on locally unfavourable slopes.

A 'worst case' scenario is simulated by forcing all cosmic rays to interact with unfavourable local slopes, as described in James & Protheroe (2009b), thereby putting a lower bound on the emission, whereas the standard simulation assumes a random surface slope. The reality is expected to be somewhat closer to the 'random slope' calculation, since only at very low angles of incidence will large-scale surface features affect the interaction geometry. Therefore, only the mildly optimistic method is treated here.

4.1 FAST Receivers

The sensitivity of FAST is simulated assuming three receivers. The first is the planned 19-receiver multibeam with intra-beam spacing of $6.2'$, calculated by scaling the $29.1'$ spacing of the Parkes multibeam by 64/300 (the ratio of telescope diameters). Each beam was modelled as having a left circular polarisation/right circular polarisation (LCP/RCP) receiver with $T_{\rm sys} = 25\,{\rm K}$, pointed at the Moon as shown in Figure 4. Such circularly-polarised receivers cannot be aligned to take advantage of the expected radial linear polarisation of Askaryan signals. This particular configuration has not been optimised, but the placement of four beams very close to the lunar limb should be close to optimum. Airy beams appropriate to a 300 m aperture were assumed, with an effective area of $50\,000\,{\rm m}^2$ per beam (equivalent to 70% aperture efficiency). The observation band was $1.23 - 1.53\,{\rm GHz}$, with the contribution of lunar thermal noise integrated for each beam across this band, assuming a lunar blackbody temperature of 225 K. The detection criteria assumed a simple voltage threshold trigger requiring a coincidence in both the RCP and LCP channels of a single beam at 5.9 times that of the thermal noise, for a double-coincidence rate off pure noise of five times per year for all 19 beams. Perfect correction for ionospheric dispersion and instrumental effects, and perfect discrimination against RFI, is also assumed. While obviously unrealistic for a real-time trigger, such sensitivity is feasible in offline analysis, provided the real-time trigger threshold is set sufficiently low.

The second receiver considered is the proposed broadband SPF, operating from 270 MHz to 1.45 GHz, but otherwise identical to the multibeam receivers. For this simpler configuration, several pointing positions near the lunar limb were simulated, representing different trade-offs between reduced lunar noise from off-limb pointing and a corresponding reduction in sensitivity to signal events. It was found that the optimal pointing position was $0.5'$ off the lunar limb, which is the pointing position shown in Figure 4.

The third receiver considered is a PAF of sufficient size to cover the entire lunar surface with an effective area of $50\,000\,{\rm m}^2$. A base $T_{\rm sys}$ of 50 K was used, to which was added 225 K of lunar emission. Dual linear polarisations were assumed for this PAF, with an either-or detection threshold of 8.6 times the thermal noise in each polarisation channel. Note that the linearly-polarised receivers will interact with the radial linear polarisation of the signal to create a non-radially-symmetric sensitivity about the lunar limb. The ASKAP PAF is sensitive to the frequency range of 700 MHz–1.8 GHz, all of which could be digitised and used simultaneously in a UHE particle search. Therefore, this is the bandwidth chosen for the simulated PAF on FAST. Sufficiently many beams to cover the entire lunar disc were assumed.

Together, these three options represent a range of trade-offs from high-sensitivity, low-coverage observations (the SPF), through medium-sensitivity, medium-coverage observations (the multibeam), to low-sensitivity, high-coverage observations (PAF), although the broad bandwidth of the PAF will make it more sensitive to Askaryan pulses than the multibeam. All three were applied to the simulated radio signals from cosmic ray and neutrino interactions in the Moon.

4.2 Sensitivity to Cosmic Rays

The corresponding effective apertures to cosmic rays from the receivers described in Section 4.1 are shown in Figure 6. The implications of receiver choice are clear: a broadband PAF, able to view the entire Moon with close to full sensitivity, provides a much higher sensitivity over the full cosmic ray energy range than either the SPF or the multibeam. While the SPF may have a marginally broader bandwidth and lower system temperature, the ability to view the entire Moon is of paramount importance. It is only above 10^{20} eV, where a cosmic-ray signal becomes strong enough to enter through the sidelobes of the SPF, that the effective area is more than 10% that of a PAF. For all receivers simulated, the detection threshold for FAST is approximately 10^{19} eV, and thus the telescope should be sensitive to the full energy range at which the cosmic-ray arrival direction contains information.

In order to determine the event rate, the apertures of Figure 6 have been convolved with the approximate cosmic-ray flux measured by the Pierre Auger Observatory (The Pierre Auger Collaboration 2013). The results are shown in Figure 7. Combining the very steep cosmic-ray

spectrum (no harder than $dN/dE \sim E^{-3}$) with the sharp turn-on of the effective experimental aperture above the threshold produces a sensitivity which is sharply peaked and spans only a relatively small energy range. The peak flux is expected between $2-3\times10^{19}$ eV, depending on the receiver. The integrated event rates for the multibeam, SPF and PAF are 48, 55 and 630 events per full year's worth of observation respectively, while the rates of 'interesting' events with energies above 5.6×10^{19} eV are 2, 3 and 39 per year (the rate for the Pierre Auger Observatory is approximately 30 per year).

From the estimates in Figure 7, a PAF on FAST would detect approximately one event per two six-hour observations; equivalently, a month spent tracking the Moon whenever it is visible should yield of the order of fifteen events. In the extreme energy range above 5.6×10^{19} eV where cosmic ray arrival directions carry useful information on the source flux, the event rate — adjusted for a lunar visibility of perhaps 25% — is ten per year. While this rate is not sufficient to compete directly with the Pierre Auger Observatory, it raises the prospect of FAST making a first detection using the lunar Askaryan technique, thereby paving the way for instruments such as the SKA to make even-more-sensitive observations.

The total number of cosmic-ray detections is not the only experimental outcome however. The particular geometry of lunar Askaryan emission means that different observation modes will be sensitive to different parts of the sky (James & Protheroe 2009a). The instantaneous effective area to cosmic rays of 5×10^{19} eV for both the FAST SPF and PAF is shown in Figure 8 as a function of their arrival direction relative to the Moon. In the case of the PAF, which is assumed to view the entire Moon, the coverage is radially symmetric about the lunar centre, and is distributed in a broad band between approximately 15° and 40° from the Moon. The coverage of the SPF is maximal in a region of approximate dimensions $30^\circ\times70^\circ$, centred $\sim20^\circ$ from the Moon in the direction given by the beam-pointing position on the lunar limb. Thus these two modes have not only different energy-dependencies for their sensitivity — they also have different angular-dependencies as well. Note that the directional sensitivity dependence means that by scheduling observations when the Moon is in a part of the sky near a candidate UHE particle source (such as Centaurus A), the low fraction of telescope observation time compared to the 100% duty cycle of an experiment such as the Pierre Auger Observatory can be somewhat compensated for (James et al., 2011b).

4.3 Sensitivity to Neutrinos

The effective aperture to UHE neutrinos of the three receiver packages is given in Figure 9. The shape is quite different from that of cosmic rays, due to the different interaction phenomenology of the particles. Since the majority of neutrinos interacts too deeply for their radiation to escape the surface, and only a fraction of their energy is given to hadronic cascades, the total effective aperture of the simulated FAST receivers for UHE neutrinos is much lower than for UHE cosmic rays. This is why the aperture continues to increase with energy: particles with higher energy can be detected at greater depths and when giving a lower fraction of their energy to hadronic cascades. Thus at extreme energies above 10^{22} eV, the SPF is more sensitive to UHE neutrinos than the PAF, since its lower system temperature and lower minimum frequency allow it to probe more deeply into the Moon. Additionally, since neutrinos can penetrate a significant fraction of the lunar limb, and thus undergo interactions that point out of the surface, it becomes possible to detect the peak emission at high frequencies where the emission cone is relatively narrow. Hence, the PAF has a greater sensitivity than the SPF to particles at 'low' energies below 10^{21} eV. Given the spectral downturn in the cosmic ray spectrum near $10^{19.5}$ eV, this suggests the PAF as the optimum receiver for UHE neutrino searches as well as for UHE cosmic rays.

While no neutrino in the UHE energy range has been detected (those observed by IceCube had interaction energies of at most a few 10^{15} eV (IceCube Collaboration 2013), so that IceCube limits the flux above 10^{16} eV), several experiments have already searched for them and placed limits on their flux. As well as the Pierre Auger experiment, two radio-detection experiments have used the Antarctic ice sheet as an interaction medium to search for Askaryan pulses from UHE neutrinos. These were ANITA (Gorham et al. 2012), which consists of an array of broadband receivers mounted on a high-altitude balloon, allowing a very large volume of ice to be observed; and RICE (Kravchenko et al. 2012), which was an array of radio receivers embedded in the ice sheet itself. The limits from ANITA are expected to strengthen upon publication of results from the ANITA III flight.

The limits on UHE neutrino flux that would result from a dedicated 1000-h observation campaign with the FAST PAF or SPF are compared to existing experimental limits in Figure 10. While the limits would be competitive in the highest-energy range with those of experiments such as RICE and ANITA, a much longer observation campaign would be required in order to improve upon them. UHE

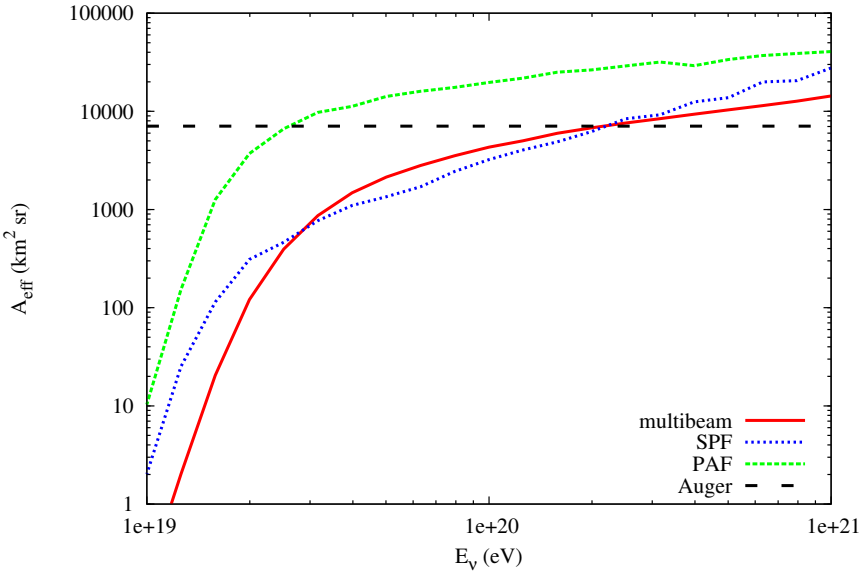

Fig. 6 Simulated effective apertures of different FAST receivers (19-beam 'multibeam', single-pixel feed 'SPF' and a phased-array feed 'PAF') to cosmic rays. Also shown for comparison is the instantaneous aperture of the Pierre Auger Observatory, which is constant in this energy range.

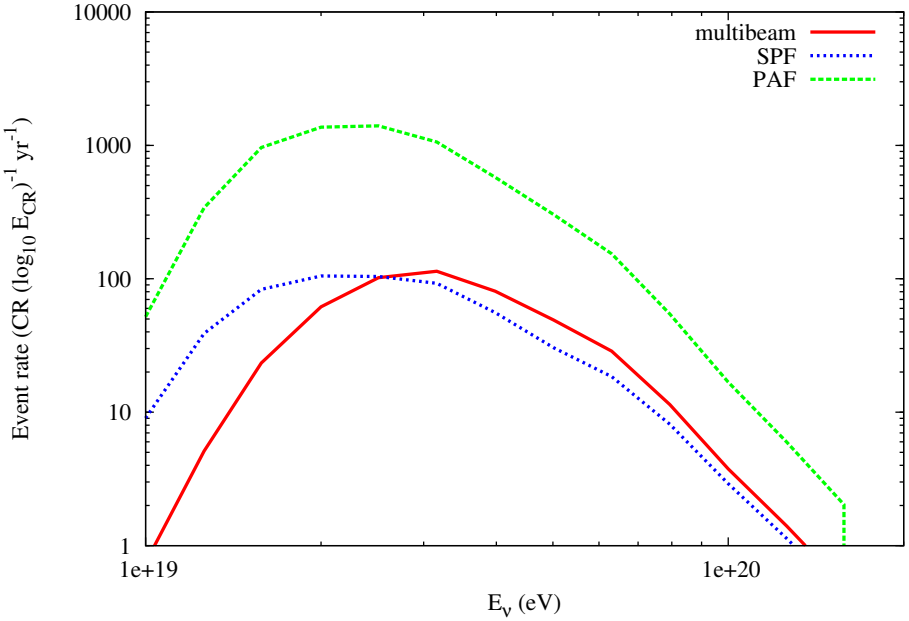

Fig. 7 Expected cosmic-ray detection rate for the FAST observations. Values above 2×10^{20} cannot be calculated, because the flux at these energies is unknown.

neutrino detection would also necessarily involve discriminating against UHE cosmic ray events, which would be detected more commonly.

5 DISCUSSION

The estimated sensitivities of UHE particle experiments with FAST calculated in Section 4 are significantly higher than any previous experimental sensitivity using the lunar Askaryan technique. The achievable limits on a UHE neutrino flux show no significant improvement upon those from the best existing experiments, in particular ANITA and RICE, which were specialised experiments designed specifically to search for UHE neutrinos. The expected rate of cosmic ray detections, once the fraction of time at which

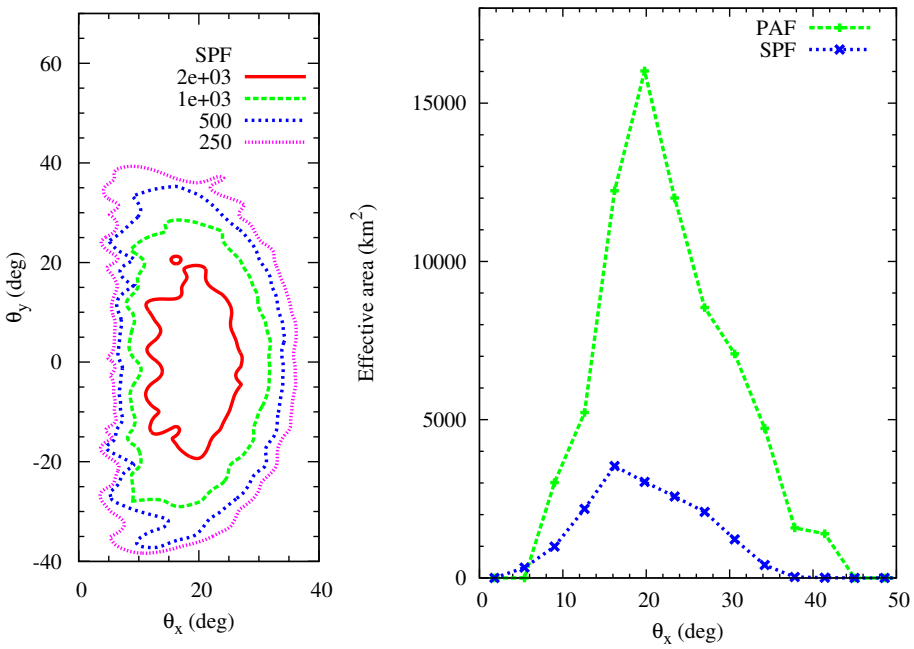

Fig. 8 Effective area (km^2) to cosmic rays of $E_{\rm CR} = 10^{19.5}$ eV as a function of their arrival direction relative to the Moon. Here, θ_x and θ_y are angles from the Moon in the x and y directions respectively in the sky plane, defined with the Moon located at (0,0) and the SPF pointing at $(x, y) = (0.27, 0)$. Left: contour plot of the effective area of the SPF; Right: one-dimensional comparison of the SPF with the PAF along the $\theta_y = 0$ line. Note that the effective area of the PAF is almost radially symmetric due to the uniform coverage of the lunar surface.

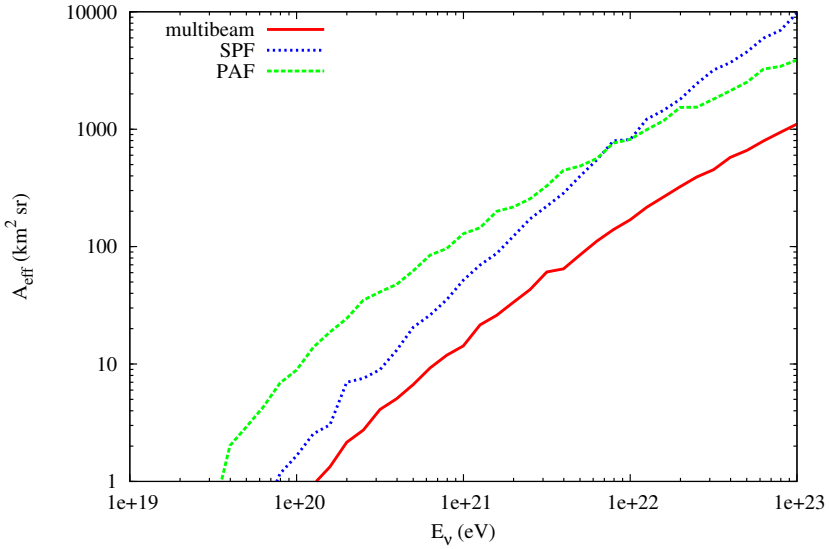

Fig. 9 Simulated effective apertures of different FAST receivers (19-beam 'multibeam', single-pixel feed 'SPF' and a phased-array feed 'PAF') to UHE neutrinos.

the Moon will be visible to FAST is taken into account, is lower than that of the existing 3000 km^2 Pierre Auger Observatory. This makes it clear that FAST will not be a long-term observatory for UHE particles.

The above results however do point towards a very clear goal of FAST: to make the first detection of a UHE particle using the lunar Askaryan technique. The outcome of such a campaign should be to detect 'a few' lunar UHE particle events, regardless of their nature, and thereby

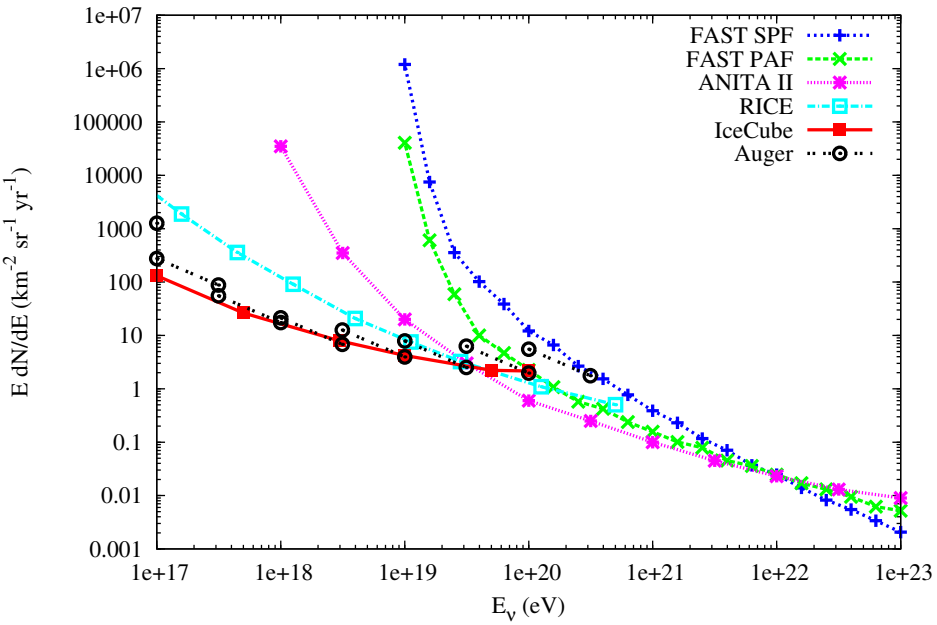

Fig. 10 Limits on the UHE neutrino flux which would arise from a 1000 h observation campaign with FAST, using the PAF or SPF, compared to existing limits from the ANITA II balloon flight (Gorham et al. 2012), RICE (Kravchenko et al. 2012), IceCube (Aartsen et al. 2016; Aartsen & Aartsen 2017) and the Pierre Auger Observatory (Aab et al. 2015). Limits have been scaled to apply to fluxes spanning a factor of e in E_ν.

demonstrate that the lunar Askaryan technique is feasible. This could be achieved with the known cosmic ray flux using a broadband PAF in as little as one week's worth of observations (seven six-h periods). For the SPF or the multibeam, a much longer campaign of several months' duration would be required. Such a detection would be a major milestone in both astroparticle physics and radio astronomy in general, and of course the FAST telescope itself, and pave the way for even more sensitive observations with the SKA (Bray et al. 2015).

The major limits to the sensitivity of such observations will be the effects of surface roughness, the ability to reject RFI, and whether or not a broadband PAF is built for FAST.

The exact effects of lunar surface roughness on the radio signal from UHE particle cascades below the surface are not yet known. This is particularly important for cosmic-ray detection, since the initial interactions of these particles are sensitive to large-scale features. Recent work has shown that it is possible to model the effects of small-scale roughness on the propagation of coherent radio pulses from particle cascades (James 2012), while detailed maps of the large-scale lunar surface are also available. It is vital that this work be continued, and this source of uncertainty be removed.

RFI rejection, which must be performed with high fidelity in order to identify lunar Askaryan pulses, is much more difficult on a single antenna than on a telescope array. Numerous methods exist to do this, as discussed in Section 3. However, the degree of signal purity required to confirm a detection is somewhat higher than that to set a limit. Experience has also shown that it is difficult to anticipate the nature of the nanosecond-scale RFI environment. The successful methods employed to reject RFI by the LUNASKA collaboration in their recent experiment at Parkes (Bray et al. 2013b) indicate that complete RFI rejection is indeed possible with a multibeam receiver, and hence also with a PAF. It is unlikely however that an SPF would be able to achieve this goal.

The building of a broadband PAF with capabilities matching those modelled (700 MHz to 1.8 GHz bandwidth) will pose a significant challenge. In particular, covering the entire Moon to half-power sensitivity at 1.8 GHz (beam width $2'$) would require over 200 beams to be formed. Since most of the signal will originate from the lunar limb due to the limb-brightening effects, forming beams to cover the limb would capture most of the signal — additionally, the system noise for these beams would be reduced. A preliminary simulation of such a configuration indicates that when using $24 - 36$ beams (with spacing of half power beamwidth (HPBW) at 870 MHz and 1.3 GHz respectively), the reduced lunar noise compensates completely for the imperfect lunar coverage. Therefore, the

highly promising simulation results for the PAF may indeed be achievable in practise.

6 CONCLUSIONS

We have described how FAST, using the lunar Askaryan technique to search for nanosecond pulses of radiation, could detect the flux of UHE cosmic rays and potentially UHE neutrinos. Using the planned L-band multibeam receiver, the known cosmic ray flux could be detected in a few months' of observation time, making FAST the first such telescope to do so. A PAF capable of forming 24 beams over a 700 MHz to 1.8 GHz bandwidth would make FAST a far superior instrument for such observations, allowing the flux to be detected in as little as a week.

Using the lunar Askaryan technique with FAST would be technically challenging and very different from the usual telescope observation modes. The techniques of signal detection and RFI rejection developed for the LUNASKA observations with the Parkes multibeam have demonstrated that such observations are possible however with a single large antenna, allowing the theoretical sensitivity limit of telescope system temperature to be reached. On the theoretical side, advances in the understanding of the effects of lunar surface roughness are required in order to reduce the uncertainty in the event rate, and improved estimates of the achievable angular and energy resolution should be made, although the expectation is that these will not achieve the accuracy of experiments such as the Pierre Auger Observatory.

The promise of the lunar Askaryan technique with FAST is such that both technical and theoretical efforts would be well-justified, and would allow FAST to become the first terrestrial telescope to successfully utilise the lunar Askaryan technique.

References

Aab, A., Abreu, P., Aglietta, M., et al. 2015, Phys. Rev. D, 91, 092008

Aartsen, M. G., Abraham, K., Ackermann, M., et al. 2016, Physical Review Letters, 117, 241101

Aartsen, M. G., & Aartsen, M. G. 2017, Physical Review Letters, 119, 259902

Abreu, P., Aglietta, M., Ahn, E. J., et al. 2010, Astroparticle Physics, 34, 314

Alvarez-Muñiz, J., Marqués, E., Vázquez, R. A., & Zas, E. 2006, Phys. Rev. D, 74, 023007

Alvarez-Muñiz, J., & Zas, E. 1998, Physics Letters B, 434, 396

Askaryan, G. 1962, Sov. Phys. JETP, 14, 441

Askaryan, G. 1965, Sov. Phys. JETP, 48, 988

Beresinsky, V. S., & Zatsepin, G. T. 1969, Physics Letters B, 28, 423

Beresnyak, A. R., Dagkesamanskii, R. D., Zheleznykh, I. M., Kovalenko, A. V., & Oreshko, V. V. 2005, Astronomy Reports, 49, 127

Bray, J. D. 2016, Astroparticle Physics, 77, 1

Bray, J. D., Ekers, R. D., Roberts, P., et al. 2012, Nuclear Instruments and Methods in Physics Research A, 662, S95

Bray, J. D., Ekers, R. D., & Roberts, P. 2013a, Experimental Astronomy, 36, 155

Bray, J. D., Ekers, R. D., Protheroe, R. J., et al. 2013b, in American Institute of Physics Conference Series, 1535, eds. R. Lahmann, T. Eberl, K. Graf, C. James, T. Huege, T. Karg, & R. Nahnhauer, 21

Bray, J., Alvarez-Muniz, J., Buitink, S., et al. 2015, in Proc. Advancing Astrophysics with the Square Kilometre Array (AASKA14), 144

Buitink, S., Scholten, O., Bacelar, J., et al. 2010, A&A, 521, A47

Dagkesamanskii, R. D., & Zheleznykh, I. M. 1989, Pisma v Zhurnal Eksperimentalnoi i Teoreticheskoi Fiziki, 50, 233

Gandhi, R., Quigg, C., Reno, M. H., & Sarcevic, I. 1998, Phys. Rev. D, 58, 093009

Gayley, K. G., Mutel, R. L., & Jaeger, T. R. 2009, ApJ, 706, 1556

Gorham, P. W., Allison, P., Baughman, B. M., et al. 2012, Phys. Rev. D, 85, 049901

Gorham, P. W., Hebert, C. L., Liewer, K. M., et al. 2004, Physical Review Letters, 93, 041101

Hankins, T. H., Ekers, R. D., & O'Sullivan, J. D. 1996, MNRAS, 283, 1027

IceCube Collaboration. 2013, Science, 342, 1242856

Jaeger, T. R., Mutel, R. L., & Gayley, K. G. 2010, Astroparticle Physics, 34, 293

James, C. W. 2012, Nuclear Instruments and Methods in Physics Research A, 662, S12

James, C. W., Ekers, R. D., Álvarez-Muñiz, J., et al. 2010, Phys. Rev. D, 81, 042003

James, C. W., & Protheroe, R. J. 2009a, Astroparticle Physics, 31, 392

James, C. W., & Protheroe, R. J. 2009b, Astroparticle Physics, 30, 318

James, C. W., Falcke, H., Huege, T., & Ludwig, M. 2011a, Phys. Rev. E, 84, 056602

James, C. W., Protheroe, R. J., Ekers, R. D., et al. 2011b, MNRAS, 410, 885

Kravchenko, I., Hussain, S., Seckel, D., et al. 2012, Phys. Rev. D, 85, 062004

Li, D., Nan, R., & Pan, Z. 2013, in IAU Symposium, 291, Neutron Stars and Pulsars: Challenges and Opportunities After 80 Years, ed. J. van Leeuwen, 325

McFadden, R., Ekers, R., & Roberts, P. 2012, Nuclear Instruments and Methods in Physics Research A, 662, S234

Nan, R., Li, D., Jin, C., et al. 2011, International Journal of Modern Physics D, 20, 989
Noll, C. E. 2010, Advances in Space Research, 45, 1421
Olhoeft, G. R., & Strangway, D. W. 1975, Earth and Planetary Science Letters, 24, 394
Pierre Auger Collaboration 2007, Science, 318, 938
Pierre Auger Collaboration 2017, Science, 357, 1266
Saltzberg, D., Gorham, P., Walz, D., et al. 2001, Physical Review Letters, 86, 2802
Shkuratov, Y. G., & Bondarenko, N. V. 2001, Icarus, 149, 329
The Pierre Auger Collaboration. 2013, arXiv:1307.5059
Troitskij, V. S., & Tikhonova, T. V. 1970, Izvestiia Vysshaia Uchebn. Zaved., Radiofizika, 13, 1272
Zas, E., Halzen, F., & Stanev, T. 1992, Phys. Rev. D, 45, 362